Pergamon

Int. J. Solids Structures Vol. 35, No. 20, pp. 2617–2637, 1998

0020-7683/98 $19.00 + .00

PII: S0020-7683(97)00180-7

TORSIONAL WAVE PROPAGATION IN REINFORCED CONCRETE COLUMNS

HIDENORI MURAKAMI* and JUNYA YAMAKAWA
Department of Applied Mechanics and Engineering Sciences, University of California at San Diego, La Jolla, California 92093-0411, U.S.A.

(*Received* 24 *September* 1996; *in revised form* 30 *December* 1996)

Abstract—Using a semi-analytical finite element (FE) method, the torsional phase velocity spectra of elastic waves were investigated for reinforced concrete (RC) columns with and without exterior composite layers. An examination of the spectra of these two types of columns shows that the retrofitted columns have a slightly smaller phase velocity in their first mode. In addition, the first mode shapes exhibit marked warping induced by the vertical bars.

Comparisons of the exact phase velocity of the first mode with those calculated from elementary theories indicate that the elementary theories give a poor prediction of the torsional wave speed even at the long wavelength limit. This inaccuracy, which comes from not including the effect of warping, can be overcome by computing the torsional rigidity utilizing Saint-Venant's semi-inverse method for torsional warping.

INTRODUCTION

The subject of torsional wave propagation in heterogeneous beams, such as reinforced concrete (RC) columns, has not been addressed prior to this work due to the complexity induced by the heterogeneity. The objectives of the present paper are: (i) to compute the torsional phase velocity spectra of columns with and without exterior composite layers (these layers have a softer shear modulus than concrete) and (ii) to examine the accuracy of elementary torsion theory in simulating torsional wave propagation.

Wave propagation in an isotropic cylinder with a uniform circular cross section was investigated by Chree (1889), Bancroft (1941), Owen (1950), and Davies (1956). The phase velocity of the first torsional mode was found to be independent of wavelength, i.e., nondispersive. For uniform beams with rectangular cross section, Barr (1962) reported that all modes were dispersive. According to Barr's experiments, torsional phase velocity of the first mode increased as wave number increased (and wavelength reduced).

Torsional wave propagation in composite circular cylinders having isotropic constituents was investigated by Armenakas (1965), Reuter (1969), Haines and Lee (1971), and Kaul *et al.* (1981).

Semi-analytical finite element methods were employed for wave-guide problems by Nelson *et al.* (1971), and Rattanawangcharoen *et al.* (1992) to investigate wave propagation in laminated-composite circular cylinders whose radial region was discretized into one-dimensional, two-node elements.

In this paper, torsional wave analyses were presented for RC columns with uniform cross section. Due to the extremely low volume fractions of spirals or tie bars, transverse reinforcement was neglected in the present investigation. It was found that the first torsional mode is nondispersive for circular, octagonal, and square cross sections irrespective of retrofitting (for the thickness of the carbon/epoxy layer considered). The elementary torsion theory fails to predict the torsional wave speed at the long wavelength limit. This inaccuracy stems from not including the effect of warping observed in the first torsional mode shapes (there is warping even in columns with circular cross section). In order to accurately predict the torsional wave speed by utilizing the elementary torsion theory, it is necessary to perform Saint-Venant's semi-inverse analysis for torsional rigidity. A finite element method was utilized to solve the boundary value problems for warping functions defined on cross

* Author to whom correspondence should be addressed.

sections (Herrmann, 1965). The torsional rigidity was also compared with the analytical and experimental results reported by Kuo and Conway (1973).

FORMULATION OF TORSIONAL WAVEGUIDE PROBLEM

Torsional wave propagation in infinitely long RC columns with uniform cross sections is considered. Cross sections of the RC columns with exterior composite layers are shown in Fig. 1. Let the x_3-axis be in the direction of the column axis, and the x_1, x_2-plane be the plane of the cross section. The x_1, x_2, and x_3 axes form a rectangular Cartesian coordinate system. Cross section Ω consists of non-overlapping sub-regions of concrete, $\Omega^{(2)}$, the exterior composite layer, $\Omega^{(3)}$, and the longitudinal steel bars, $\Omega_m^{(1)}$ ($m = 1, 2, \ldots, N$, where N denotes the number of longitudinal bars):

$$\Omega = \Omega^{(1)} \cup \Omega^{(2)} \cup \Omega^{(3)}, \quad \Omega^{(1)} = \bigcup_{m=1}^{N} \Omega_m^{(1)},$$

$$\Omega_m^{(1)} \cap \Omega^{(2)} = \varnothing, \quad \Omega^{(2)} \cap \Omega^{(3)} = \varnothing, \quad \Omega_m^{(1)} \cap \Omega_n^{(1)} = \varnothing \quad \text{if } m \neq n, \tag{1}$$

where $\varnothing$ denotes a null set, and the composite region exists only for retrofitted columns. For notational simplicity, the superscript (α) denotes variables associated with material $\alpha = 1$ (steel), 2 (concrete), and 3 (composite). The boundary of each sub-region is denoted by $\partial\Omega^{(\alpha)}$ whose unit outward normal is $n_i^{(\alpha)}$.

In what follows, Cartesian indicial notation is employed with the summation convention used for repeated indices. It is noted that due to the heterogeneity induced by steel bars, all displacement components are excited by torsional wave motion. Let $\bar{u}_i$ denote the displacement vector field, and $\bar{\varepsilon}_{ij}$, and $\bar{\sigma}_{ij}$ be the symmetric strain and stress tensor fields, respectively. The over-barred quantities denote the values in the time domain. For harmonic

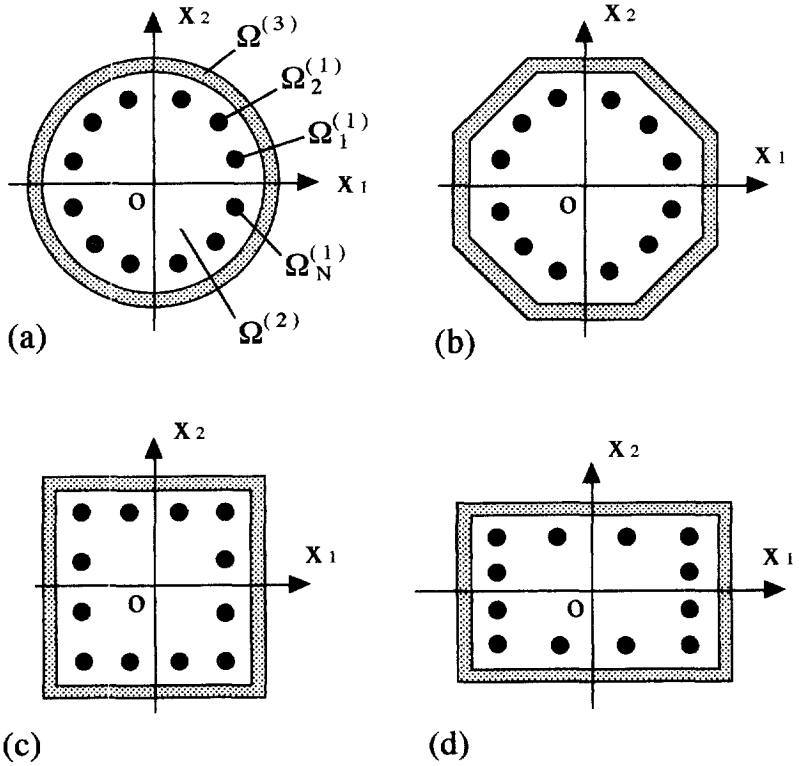

Fig. 1. Retrofitted RC columns with (a) circular, (b) octagonal, (c) square, and (d) rectangular cross sections of equal area.

motion with angular frequency ω, the displacement vector, strain tensor, and stress tensor fields take the form:

$$[\bar{u}_i \quad \bar{\varepsilon}_{ij} \quad \bar{\sigma}_{ij}](x_1, x_2, x_3, t) = [u_i \quad \varepsilon_{ij} \quad \sigma_{ij}](x_1, x_2, x_3, \omega) \exp(-\sqrt{-1}\omega t), \tag{2}$$

where t denotes time, and u_i, ε_{ij}, and σ_{ij} are complex amplitudes of displacements, strains, and stresses, respectively. The physical components of those variables are the real or imaginary part of the above quantities. For notational clarity, $\sqrt{(-1)}$ is used, instead of i, to avoid any confusion with the $i\,(=1,2,3)$ used for indicial notation.

The harmonic equations of motion become

$$\sigma^{(\alpha)}_{ji,j} + \rho^{(\alpha)}\omega^2 u^{(\alpha)}_i = 0 \quad \text{in}\,\Omega^{(\alpha)}, \tag{3}$$

where $(\,)_{,j} = \partial(\,)/\partial x_j$, and ρ is mass density.

Hooke's law is described as

$$\sigma^{(\alpha)}_{ij} = C^{(\alpha)}_{ijmn}\varepsilon^{(\alpha)}_{mn} \quad \text{in}\,\Omega^{(\alpha)}, \tag{4a}$$

where C_{ijmn} is the elastic modulus tensor.

For isotropic material 1 (steel) and material 2 (concrete) the elastic modulus tensor can be written in terms of shear modulus G and Poisson's ratio ν as:

$$\sigma^{(\alpha)}_{ij} = 2G^{(\alpha)}\left\{\frac{\nu^{(\alpha)}}{(1-2\nu^{(\alpha)})}\varepsilon^{(\alpha)}_{kk}\delta_{ij} + \varepsilon^{(\alpha)}_{ij}\right\} \quad \text{in}\,\Omega^{(\alpha)}, \quad \alpha = 1 \quad \text{and} \quad 2 \tag{4b}$$

where δ_{ij} is the Kronecker delta ($\delta_{ij} = 1$ if $i = j$, $\delta_{ij} = 0$ if $i \neq j$). The exterior composite layer is characterized as a cylindrically orthotropic material which becomes monoclinic with respect to the x_i-coordinate system (Lekhnitskii, 1963).

The strain–displacement relations are

$$\varepsilon^{(\alpha)}_{mn} = \tfrac{1}{2}(u^{(\alpha)}_{m,n} + u^{(\alpha)}_{n,m}) \quad \text{in}\,\Omega^{(\alpha)}. \tag{5}$$

The interfacial boundary conditions consist of the continuity of displacements and tractions on each interface between the steel bar and concrete, $\partial\Omega^{(1)}_m$:

$$u^{(1)}_i = u^{(2)}_i, \quad \sigma^{(1)}_{ji}n^{(1)}_j = \sigma^{(2)}_{ji}n^{(1)}_j \quad \text{on}\,\partial\Omega^{(1)}_m, \quad m = 0, 1, \ldots, N. \tag{6a,b}$$

For the columns with composite layers, the continuity conditions are prescribed on the interface between the concrete and composite layer, $\partial\Omega^{(2)}_0$:

$$u^{(2)}_i = u^{(3)}_i, \quad \sigma^{(2)}_{ji}n^{(2)}_j = \sigma^{(3)}_{ji}n^{(2)}_j \quad \text{on}\,\partial\Omega^{(2)}_0 \quad \text{if}\,\Omega^{(3)} \neq \varnothing. \tag{7a,b}$$

The traction free condition on the exterior composite surface $\partial\Omega^{(3)}_0$ becomes:

$$\sigma^{(3)}_{ji}n^{(3)}_j = 0 \quad \text{on}\,\partial\Omega^{(3)}_0 \quad \text{if}\,\Omega^{(3)} \neq \varnothing. \tag{7c}$$

For unretrofitted columns, the traction free condition holds on the boundary $\partial\Omega^{(2)}_0$:

$$\sigma^{(2)}_{ji}n^{(2)}_j = 0 \quad \text{on}\,\partial\Omega^{(2)}_0 \quad \text{if}\,\Omega^{(3)} = \varnothing. \tag{8}$$

In what follows, harmonic wave propagation with wave number k in the x_3-direction is considered. The wave number is related to the wavelength Λ as $k = 2\pi/\Lambda$. The displacement and stress fields are expressed in the form:

$$u_i^{(\alpha)}(x_1, x_2, x_3, \omega) = \tilde{u}_i^{(\alpha)}(x_1, x_2, k, \omega) \exp(\sqrt{-1}kx_3), \tag{9a}$$

$$\sigma_{ij}^{(\alpha)}(x_1, x_2, x_3, \omega) = \tilde{\sigma}_{ij}^{(\alpha)}(x_1, x_2, k, \omega) \exp(\sqrt{-1}kx_3). \tag{9b}$$

For a given wave number k, the above problem (3)–(9), defines an eigenvalue problem for angular frequencies (eigenvalues) and corresponding mode shapes. Phase velocity C_p and group velocity C_g are obtained from k and ω as (Fung 1965, Chap. 11):

$$C_p = \frac{\omega}{k}, \quad C_g = \frac{d\omega}{dk}. \tag{10a,b}$$

The above strong formulation of the problem can be cast in a variational form by utilizing Hamilton's principle (Nelson *et al.*, 1971):

$$\delta \left\{ \sum_{\alpha=1}^{3} \iint_{\Omega^{(\alpha)}} \frac{1}{2} (\rho^{(\alpha)} \omega^2 u_i^{(\alpha)} u_i^{(\alpha)*} - C_{ijmn}^{(\alpha)} \varepsilon_{ij}^{(\alpha)} \varepsilon_{mn}^{(\alpha)*}) \, dx_1 \, dx_2 \right\} = 0, \tag{11}$$

where $\delta( )$ implies the variation of ( ), and ( )* indicates the complex conjugate of ( ).

The above equation yields

$$\delta \left\{ \sum_{\alpha=1}^{3} \iint_{\Omega^{(\alpha)}} (-\delta \varepsilon_{ij}^{(\alpha)*} \sigma_{ij}^{(\alpha)} + \delta u_i^{(\alpha)*} \rho^{(\alpha)} \omega^2 u_i^{(\alpha)} + \text{c.c.}) \, dx_1 \, dx_2 \right\} = 0, \tag{12}$$

where "c.c." denotes the complex conjugate of the preceding terms.

Admissible displacements in each sub-region are continuous up to the second spatial derivatives and satisfy (6a) and (7a). Since Hamilton's principle is a displacement-based variational formulation, eqns (4) and (5) become definitions or constraints. For admissible displacement fields, the Euler–Lagrange equations of (11) yield the equations of motion, (3), the traction continuity, (6b), (7b), and the traction free condition on the exterior boundary, (7c) or (8).

In this paper, cross sections with double axes of symmetry are considered (see Fig. 1). For torsional wave motion, the anti-symmetry condition is described on both the x_1- and x_2-axes as:

$$\sigma_{11} = u_2 = u_3 = 0 \quad \text{on } x_1 = 0, \tag{13a,b,c}$$

$$u_1 = \sigma_{22} = u_3 = 0 \quad \text{on } x_2 = 0. \tag{14a,b,c}$$

By taking advantage of the above conditions, only one quadrant of cross section Ω needs to be analyzed. In this case, admissible displacements in each sub-region must satisfy (13b,c) and (14a,c) in addition to (6a) and (7a).

SEMI-ANALYTICAL FINITE ELEMENT ANALYSES

By taking advantage of the antisymmetry conditions (13) and (14), only one quadrant of cross section Ω needs to be discretized into four-node quadrilateral elements. The

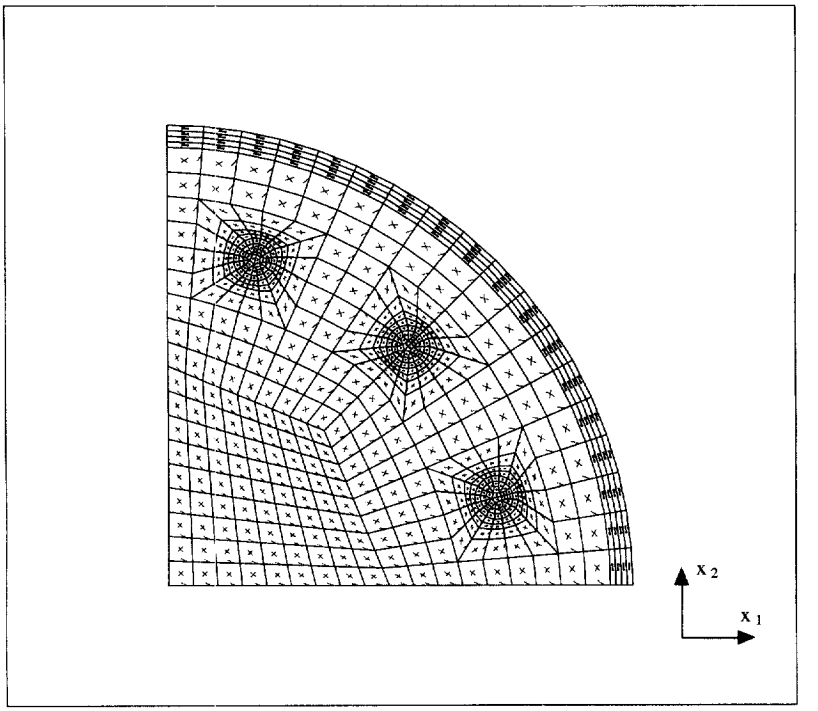

Fig. 2. A representative finite element mesh.

representative mesh used for numerical analyses is shown in Fig. 2. Each node has three translational degrees-of-freedom in complex form. Non-overlapping finite-element regions are denoted by $\Gamma^{(e)}$, $e = 1, 2, \ldots, N_{el}$:

$$\Omega = \bigcup_{e=1}^{N_{el}} \Gamma^{(e)}, \quad \Gamma^{(e)} \bigcap \Gamma^{(f)} = \varnothing \quad \text{if } e \neq f, \tag{15}$$

where N_{el} is the total number of elements.

In a typical isoparametric element, $\Gamma^{(e)}$, the displacement field is approximated by nodal displacements (Hughes, 1987):

$$\{u\}^{(e)} = [N]^{(e)}\{\tilde{U}\}^{(e)} \exp(\sqrt{-1}kx_3) \quad \text{in } \Gamma^{(e)}, \tag{16a}$$

where $\{u\}$ is the 3×1 displacement matrix:

$$\{u\}^{(e)} = [u_1^{(e)} \quad u_2^{(e)} \quad u_3^{(e)}]^T, \tag{16b}$$

$[N]$ is the 3×12 interpolation matrix, and $\{U\}$ represents the complex 12×1 nodal displacement matrix. These matrices are defined in Appendix A. In (16b), the superscript "T" represents the transpose.

The strain–displacement relation (5) together with (16) becomes in matrix form:

$$\{\varepsilon\}^{(e)} = [B]^{(e)}\{\tilde{U}\}^{(e)} \exp(\sqrt{-1}kx_3) \quad \text{in } \Gamma^{(e)}, \tag{17a}$$

where $\{\varepsilon\}$ is the 6×1 strain matrix:

$$\{\varepsilon\}^{(e)} = [\varepsilon_{11}^{(e)} \quad \varepsilon_{22}^{(e)} \quad \varepsilon_{33}^{(e)} \quad 2\varepsilon_{23}^{(e)} \quad 2\varepsilon_{31}^{(e)} \quad 2\varepsilon_{12}^{(e)}]^T, \tag{17b}$$

and $[B]$ is the complex 6×12 strain–displacement matrix, defined in Appendix A.

Hooke's law (4) is rewritten in matrix form as:

$$\{\sigma\}^{(e)} = [D]^{(e)}\{\varepsilon\}^{(e)} \quad \text{in } \Gamma^{(e)}, \tag{18a}$$

where $\{\sigma\}$ is the 6×1 stress matrix,

$$\{\sigma\}^{(e)} = [\sigma_{11}^{(e)}\sigma_{22}^{(e)} \quad \sigma_{33}^{(e)} \quad \sigma_{23}^{(e)} \quad \sigma_{31}^{(e)} \quad \sigma_{12}^{(e)}]^T, \tag{18b}$$

and $[D]$ is the 6×6 elastic modulus matrix, defined in Appendix A. The matrix $[D]$ is constructed by utilizing the appropriate elastic moduli of material α $(=1,2,3)$.

The substitution of (16)–(18) into (12) yields

$$\sum_{e=1}^{N_{el}} \iint_{\Gamma^{(e)}} (-\delta\{\varepsilon^*\}^{(e)T}\{\sigma\}^{(e)} + \omega^2 \delta\{u^*\}^{(e)T}\rho^{(e)}\{u\}^{(e)})\,dx_1\,dx_2 + \text{c.c.}$$

$$= \sum_{e=1}^{N_{el}} \delta\{\tilde{U}^*\}^{(e)T}[-[K]^{(e)}\{\tilde{U}\}^{(e)} + \omega^2[M]^{(e)}\{\tilde{U}\}^{(e)}] + \text{c.c.} = 0, \tag{19}$$

where $[K]^{(e)}$ is the element stiffness matrix, which is a 12×12 Hermitian matrix,

$$[K]^{(e)} = \iint_{\Gamma^{(e)}} [B^*]^{(e)T}[D]^{(e)}[B]^{(e)}\,dx_1\,dx_2, \tag{20a}$$

and $[M]^{(e)}$ is the element mass matrix, which is a 12×12 real symmetric matrix,

$$[M]^{(e)} = \iint_{\Gamma^{(e)}} [N]^{(e)T}\rho^{(e)}[N]^{(e)}\,dx_1\,dx_2. \tag{20b}$$

In the above derivation, the complex conjugates of the variations of (16a) and (17a):

$$\delta\{u^*\}^{(e)T} = \delta\{\tilde{U}^*\}^{(e)T}[N]^{(e)T}\exp(-\sqrt{-1}kx_3), \tag{21a}$$

$$\delta\{\varepsilon^*\}^{(e)T} = \delta\{\tilde{U}^*\}^{(e)T}[B]^{(e)T}\exp(-\sqrt{-1}kx_3), \tag{21b}$$

have been utilized.

After assembling both element stiffness and mass matrices for the global degrees-of-freedom, the Euler–Lagrange equations of (19) render an algebraic eigenvalue problem,

$$[K]\{\tilde{U}\} = \omega^2[M]\{\tilde{U}\}, \tag{22}$$

where the global stiffness matrix $[K]$ is Hermitian, $[K]^{*T} = [K]$, and the global mass matrix $[M]$ is real and symmetric, $[M]^T = [M]$. It is known that Hermitian matrices have real eigenvalues (Noble and Daniel, 1977).

In the numerical analyses, it is convenient to nondimensionalize elastic moduli and mass density by those of concrete. Spatial variables and displacements are nondimensionalized by a reference length, d, of the cross section. With this nondimensionalization, wave number, $kd = 2\pi d/\Lambda$, is prescribed and the eigenvalue problem (22), is solved numerically for eigenpairs starting from the lowest modes,

$$\left(\frac{\omega_\beta d}{C_s}, \frac{1}{d}\{\tilde{U}\}_\beta\right), \quad \beta = 1, 2, \ldots \tag{23}$$

where $C_s = \sqrt{(G^{(2)}/\rho^{(2)})}$ is the concrete shear wave velocity in a full space.

The above eigenvalue analyses were conducted using an HP workstation. The global stiffness matrix was stored in skyline format and a lumped mass matrix was employed. The lumped mass matrix was constructed based upon the row-sum algorithm (Hughes, 1987, Chap. 7). The first 15 modes were computed using the inverse iteration method with the shifting to higher modes (Hughes, 1987, Chap. 10). To this end, the existing triangularization algorithm for the skyline storage scheme of symmetric matrices was generalized for Hermitian matrices. The code was validated by computing phase velocity spectra for homogeneous beams with uniform circular cross-section and comparing the phase velocity for the (nondispersive) lowest mode with the exact value predicted by Chree (1889).

NUMERICAL RESULTS

Dispersion spectra and corresponding mode shapes were computed numerically for the RC columns shown in Fig. 1. The columns considered have: (a) circular, (b) octagonal, (c) square, and (d) rectangular (with aspect ratio 3:2) cross sections of equal area and are with or without exterior composite layers to model the columns with or without composite retrofitting. The diameter of the circular cross section is 500 mm. Each column is vertically reinforced by twelve steel bars of diameter 25 mm. The circular and octagonal cross sections had their bars arranged periodically every 30° on the circle of radius 192.5 mm. For the columns with the square and rectangular cross sections, vertical rebars were arranged four per face, as shown in Figs 1(c) and 1(d), and these columns have the same core concrete area as the column with circular cross section. Material properties employed for the calculations are shown in Table 1.

The columns considered have been retrofitted with a unidirectional carbon/epoxy composite layer of thickness 12.5 mm with the fiber in the circumferential direction. The material properties of the carbon/epoxy layer are shown in Table 2. Even though the effect of retrofitting was only investigated for the unidirectional composite layer of thickness 12.5 mm, the present formulation can be applied to any anisotropic material layer described by (4a) as long as the perfect bond condition between the column and the reinforcing layer, (7), is satisfied.

In order to describe different modes, it is convenient to employ the circumferential mode number, n, of a homogeneous cylinder with a circular cross section, whose displacements are expressed in cylindrical coordinates, r and θ, as (Gazis, 1959):

Table 1. Material properties of steel and concrete

	Steel (1)	Concrete (2)
E	210 GPa	21 GPa
G	80.8 GPa	9.1 GPa
ν	0.3	0.15
ρ	7800 kg/m^3	2300 kg/m^3

Table 2. Material properties of the carbon/epoxy layer

E_L	E_T	G_{LT}	ν_{LT}	ν_{TT}	ρ
148 GPa	9.65 GPa	4.55 GPa	0.3	0.3	1500 kg/m^3

$$u_r(r,\theta,x_3) = U_r(r)\sin n\theta \exp(\sqrt{-1}kx_3)$$
$$u_\theta(r,\theta,x_3) = U_\theta(r)\cos n\theta \exp(\sqrt{-1}kx_3)$$
$$u_z(r,\theta,x_3) = U_z(r)\sin n\theta \exp(\sqrt{-1}kx_3), \tag{24}$$

where n is an integer. In addition to the torsional modes which are defined by $n = 0$ in (24), the antisymmetric conditions on the x_3–x_1 and x_2–x_3 planes, (13) and (14), also induce the circumferential modes of even numbers $n = 2, 4, 6, \ldots$. Within each circumferential mode group identified by n, there are an infinite number of modes which are referred to as the first, second, third,... modes. In the following, modes of RC columns are distinguished, except for rectangular cross section, by using the circumferential mode number, n, of a homogeneous column with a circular cross section.

The dispersion spectra and corresponding mode shapes will be first shown for the columns before retrofitting. A dispersion relation of nondimensional frequency, (23), and phase velocity, (10a), will be shown as functions of $d/\Lambda(=kd/2\pi)$ where d is the diameter of the column and Λ is the wavelength. The phase velocity will be nondimensionalized by the shear wave velocity of concrete. Also, the effect of retrofitting on dispersion relations will be shown. Comparisons of phase velocity spectra and the corresponding first torsional mode shape will be made between the columns before and after the composite retrofitting.

For the column with circular cross section and no retrofitting, Fig. 3(a) shows dispersion relations of nondimensional frequency as a function of d/Λ for the torsional modes $n = 0$ as well as the non-axisymmetric modes $n = 2$. The dispersion relation is replotted in Fig. 3(b) in terms of phase velocity as a function of d/Λ. Figure 3(c)–(e) show the phase velocity spectra for the columns with the octagonal, square, and rectangular cross sections, respectively. For comparison, the phase velocity spectra for the circular column in Fig. 3(b) are also shown by dashed lines in Fig. 3(c)–(e). The first torsional mode in each column is nondispersive, i.e., the phase velocity is independent of d/Λ as predicted by elementary torsion theory (summarized in Appendix B). In Fig. 3(d) and (e) the phase velocity of the first torsional modes for the square and rectangular columns are about 8 and 15% smaller than that of the circular column due to the smaller torsional rigidity, while the phase velocity of the first torsional mode for the octagonal column is approximately 1% less than that of the circular column.

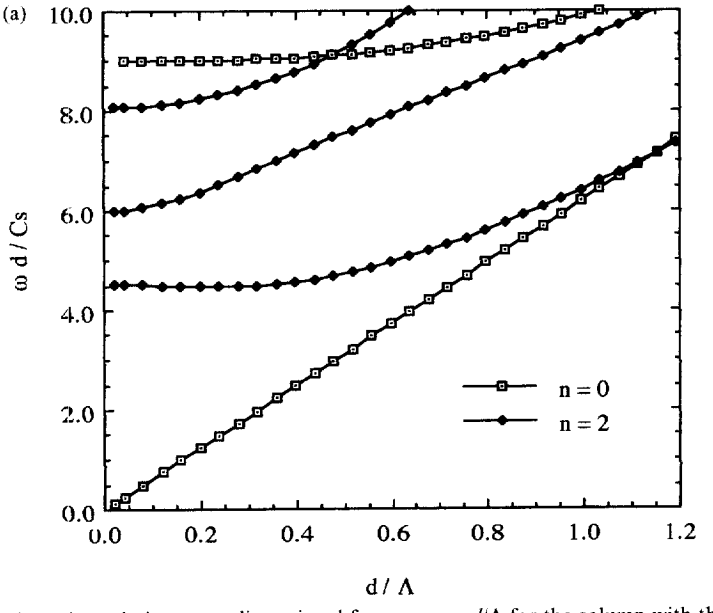

Fig. 3(a). Dispersion relations: nondimensional frequency vs d/Λ for the column with the circular cross section.

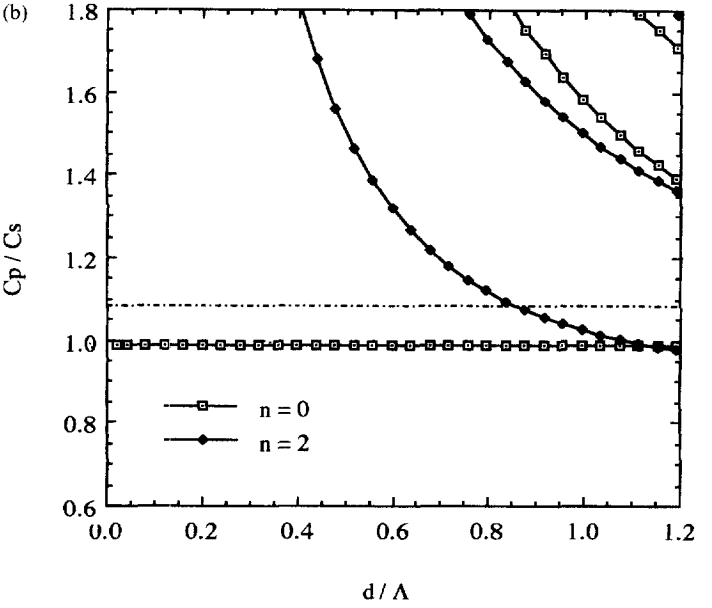

Fig. 3(b). Phase velocity vs d/Λ for the column with the circular cross section.

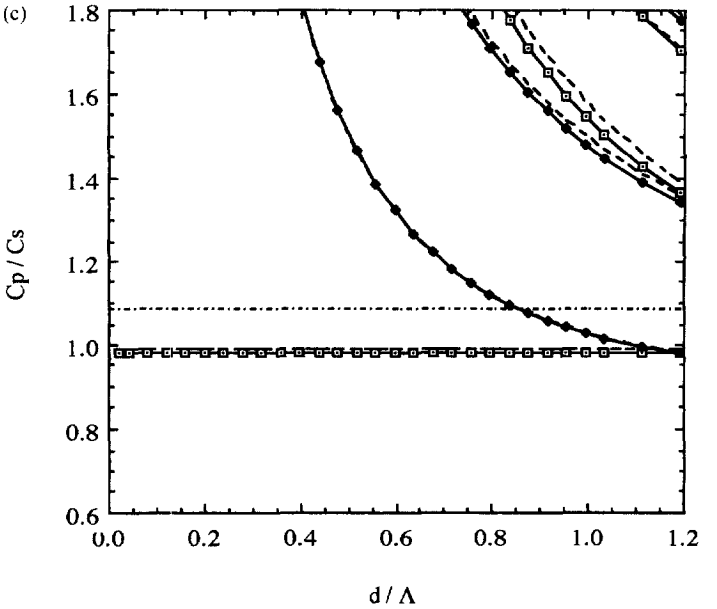

Fig. 3(c). Phase velocity vs d/Λ for the column with the octagonal cross section.

The predictions of the elementary theory of torsion, (B10) in Appendix B, are shown in Fig. 3(b)–(e) by dash–dotted lines. The elementary theory does not predict the torsional wave velocity accurately even for the columns with circular cross section.

Figure 4(a)–(d) show the first torsional mode shapes ($n = 0$, at $d/\Lambda = 0.637$) for the columns with circular, octagonal, square, and rectangular cross sections, respectively. It is known that a plane normal to the axis of a beam with a homogeneous circular cross section remains plane, i.e., no warping (Timoshenko and Goodier, 1951, 1970). Figure 4(a) shows that warping is generated, even for the column with circular cross section, by the heterogeneity induced by the reinforcing bars. The octagonal cross section in Fig. 4(b) warps in a manner similar to the circular cross section in Fig. 4(a). Considerable warping is observed for both the square and rectangular cross sections in Fig. 4(c) and (d), respectively.

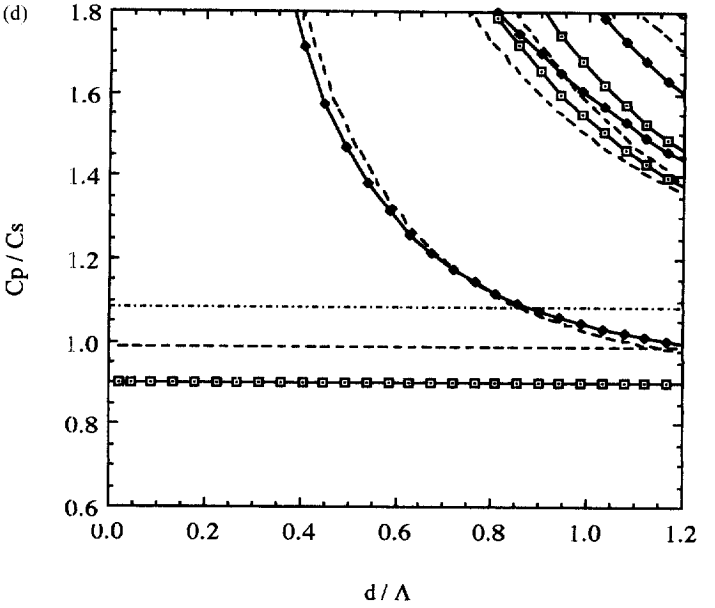

Fig. 3(d). Phase velocity vs d/Λ for the column with the square cross section.

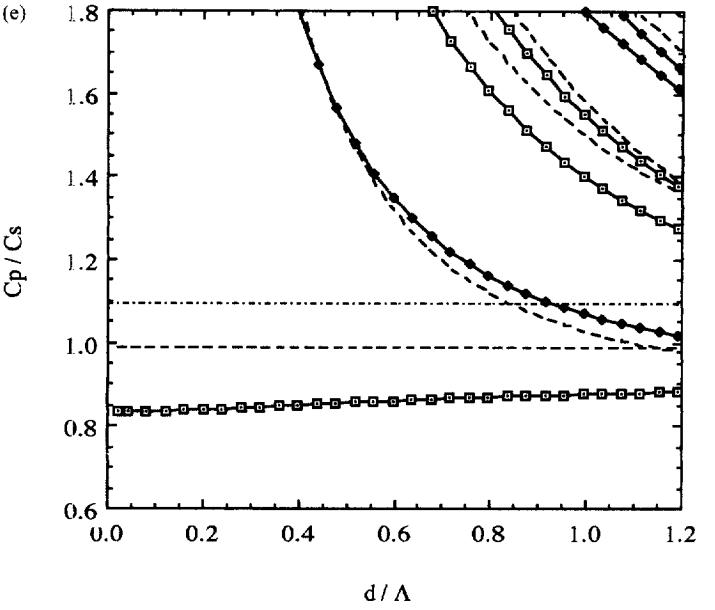

Fig. 3(e). Phase velocity d/Λ for the column with the rectangular cross section.

In Fig. 4(b)–(d), warping is observed around the steel bars and near the edges. This warping function, except for around the rebars, is approximated by that obtained for homogeneous square and rectangular cross sections (Timoshenko and Goodier, 1951, 1970). It is observed that the inaccuracy of the elementary theory in predicting torsional wave speed stems from not including the effect of warping.

For retrofitted columns, Fig. 5(a)–(d) show phase velocity spectra for torsional modes. For comparison, the phase velocity spectra of the unretrofitted RC columns in Fig. 3(b)–(e) are also shown by dashed lines. Figure 5 shows that the phase velocity spectra of the first torsional mode is slightly reduced by the exterior composite layer whose shear modulus is smaller than that of concrete.

(a)

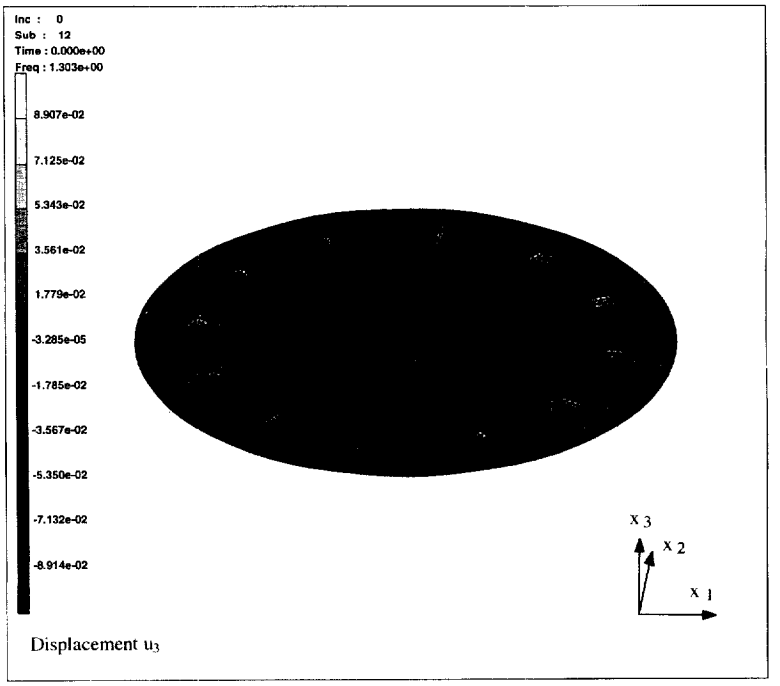

Fig. 4(a). The first torsional mode shape for the column with the circular cross section.

(b)

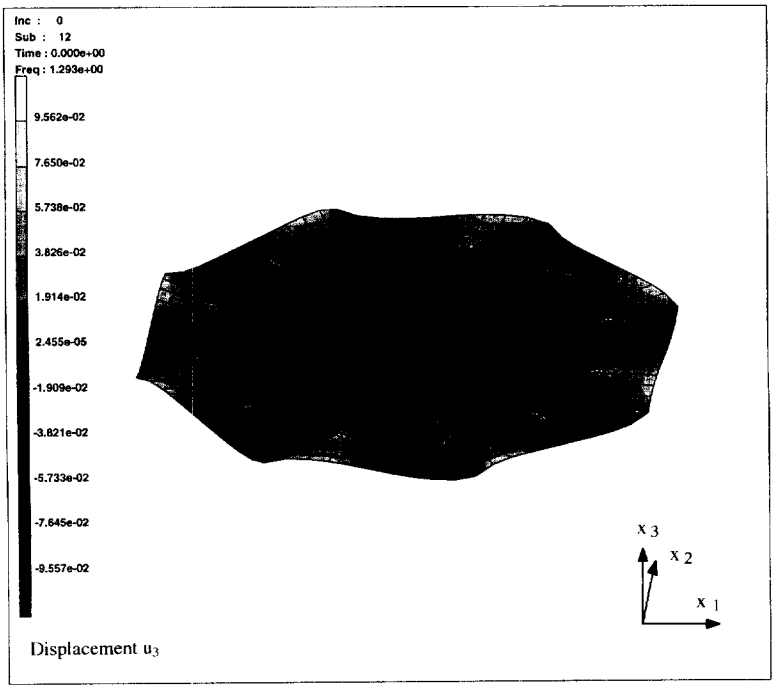

Fig. 4(b). The first torsional mode shape for the column with the octagonal cross section.

For retrofitted columns, Fig. 6(a)–(d) show the first torsional mode shapes at $d/\Lambda = 0.637$ for the circular, octagonal, square, and rectangular cross sections, respectively. These mode shapes show warping similar to that observed in Fig. 4(a)–(d). It is observed that the elementary torsion theory, (B3) and (B6), fails to simulate the torsional response of retrofitted columns even at the long wavelength limit, $d/\Lambda \to 0$.

(c)

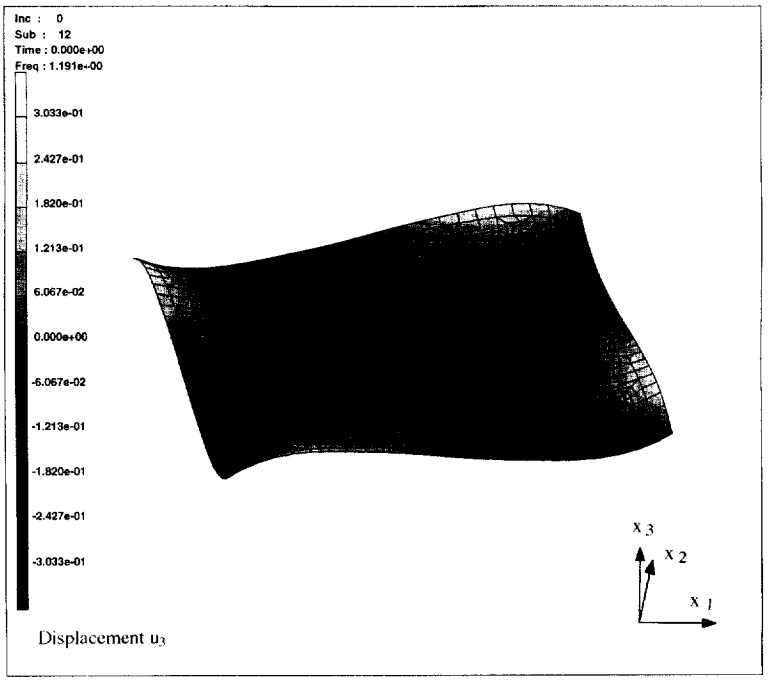

Fig. 4(c). The first torsional mode shape for the column with the square cross section.

(d)

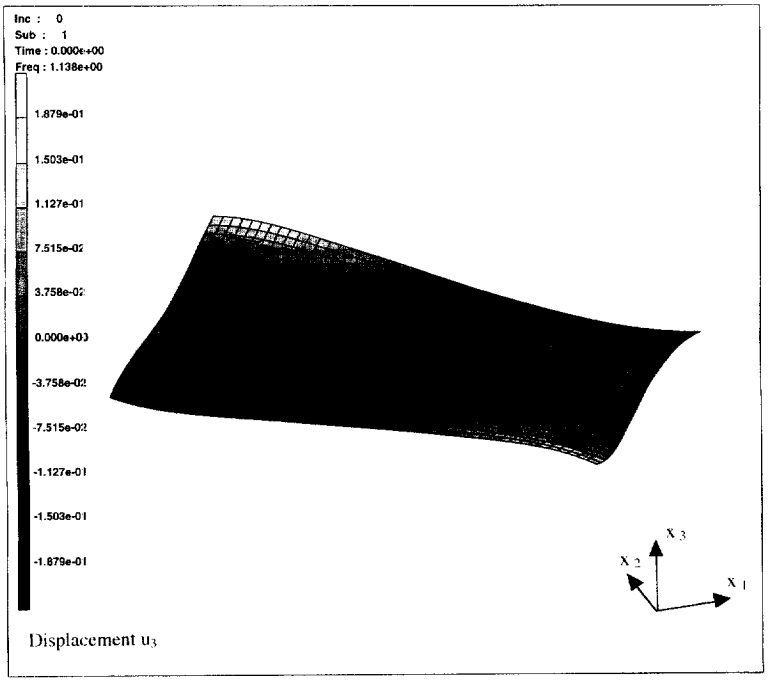

Fig. 4(d). The first torsional mode shape for the column with the rectangular cross section.

The above numerical results illustrate the need for improving the elementary torsion theory to accurately predict torsional wave speed at the long wavelength limit.

TORSIONAL RIGIDITY AND WAVE SPEED

In order to accurately predict torsional wave speed at the long wavelength limit by utilizing the elementary theory, the torsional rigidity has to be computed with the incor-

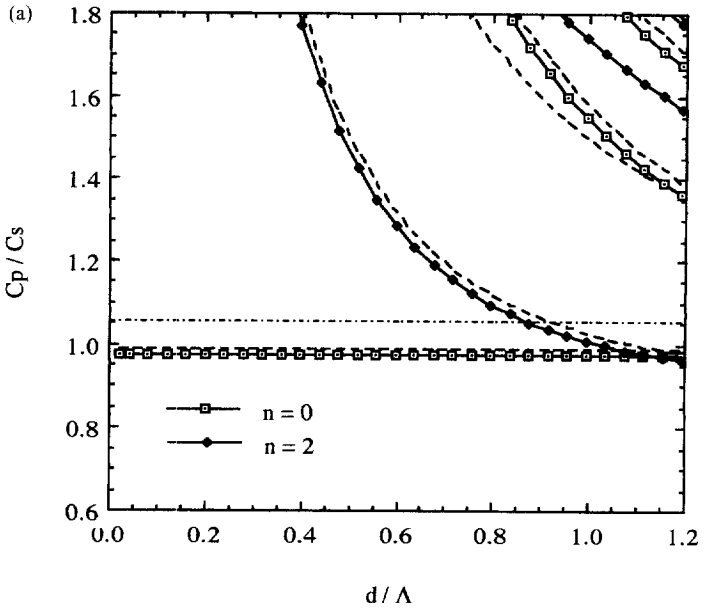

Fig. 5(a). Phase velocity vs d/Λ for the retrofitted column with the circular cross section.

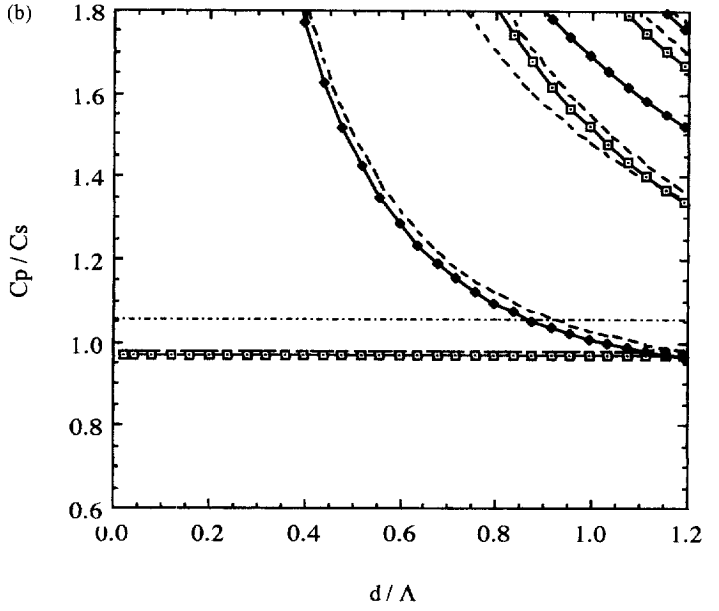

Fig. 5(b). Phase velocity vs d/Λ for the retrofitted column with the octagonal cross section.

poration of warping. To this end, Saint-Venat's semi-inverse analysis (Saint-Venant, 1856; Love, 1944) was conducted. In order to solve the boundary value problem defined on cross sections, a finite element method is utilized to obtain warping and torsional rigidity (Herrmann, 1965; Mason and Herrmann, 1968). In what follows, a semi-inverse torsional analysis is formulated for retrofitted RC columns by incorporating the heterogeneity and anisotropy for monoclinic composite layers, (A4).

Let the angle of twist per unit axial length of a cross section be denoted by ψ_3 (=constant). Saint-Venant had assumed that as the column twisted the cross sections rotated as a rigid body in the x_1, x_2-plane and warp in the x_3-direction. The column of length L is fixed at $x_3 = 0$. The displacement field takes the form:

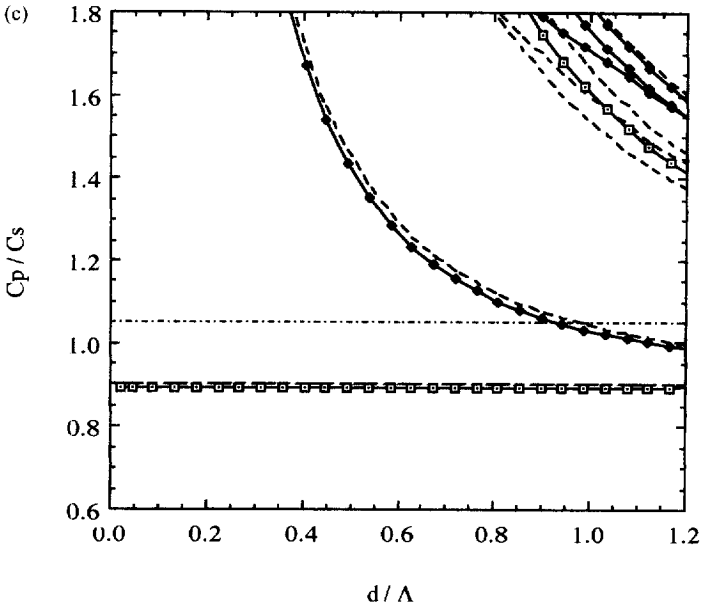

Fig. 5(c). Phase velocity vs d/Λ for the retrofitted column with the square cross section.

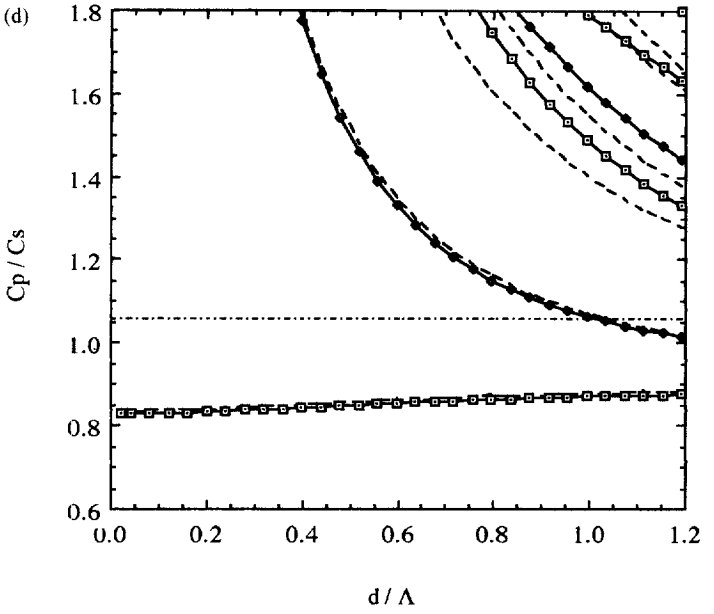

Fig. 5(d). Phase velocity vs d/Λ for the retrofitted column with the rectangular cross section.

$$
\begin{aligned}
u_1(x_1, x_2, x_3) &= -(\psi_3 x_3)x_2, \\
u_2(x_1, x_2, x_3) &= (\psi_3 x_3)x_1, \\
u_3(x_1, x_2, x_3) &= \psi_3 w(x_1, x_2),
\end{aligned} \tag{25}
$$

where $w(x_1, x_2)$ is the warping function.

A three-dimensional elastostatic boundary-value problem is defined by (3)–(5) for static problems ($\omega = 0$). The boundary conditions for the RC columns are (6)–(8) on each cross section, $x_3 =$ constant, and the end conditions are:

(a)

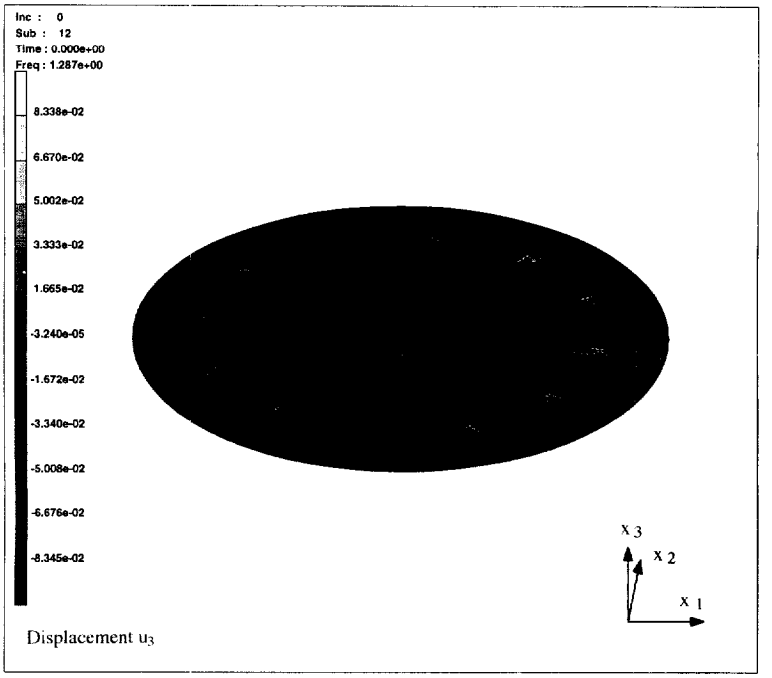

Fig. 6(a). The first torsional mode shape for the retrofitted column with the circular cross section.

(b)

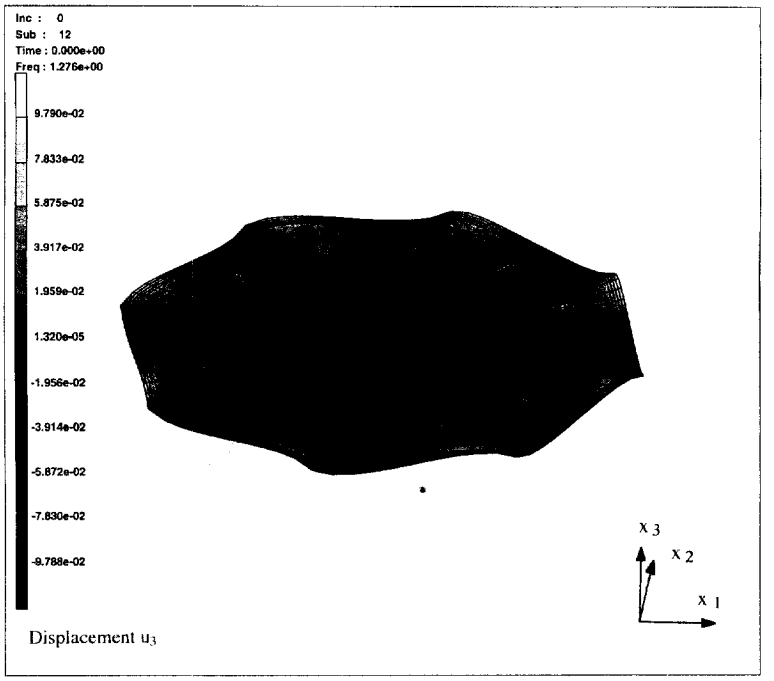

Fig. 6(b). The first torsional mode shape for the retrofitted column with the octagonal cross section.

$$u_1^{(\alpha)} = u_2^{(\alpha)} = \sigma_{33}^{(\alpha)} = 0 \quad \text{at } x_3 = 0, \tag{26}$$

$$u_1^{(\alpha)} = -(\psi_3 L)x_2, \quad u_2^{(\alpha)} = (\psi_3 L)x_1, \quad \sigma_{33}^{(\alpha)} = 0 \quad \text{at } x_3 = L. \tag{27}$$

The displacement boundary conditions, (26) and (27), render an exact elasticity solution for a three-dimensional problem and suppress the boundary layer formation investigated

(c)

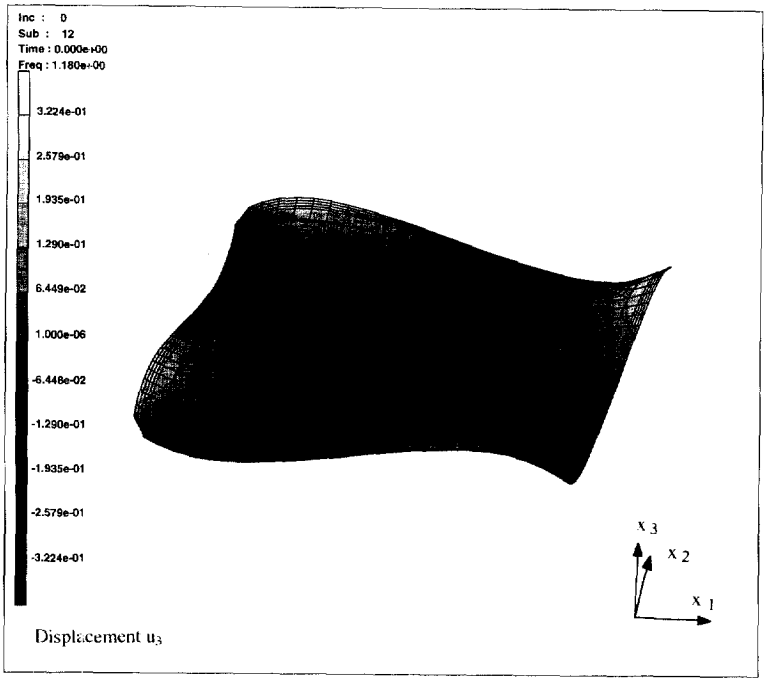

Fig. 6(c). The first torsional mode shape for the retrofitted column with the square cross section.

(d)

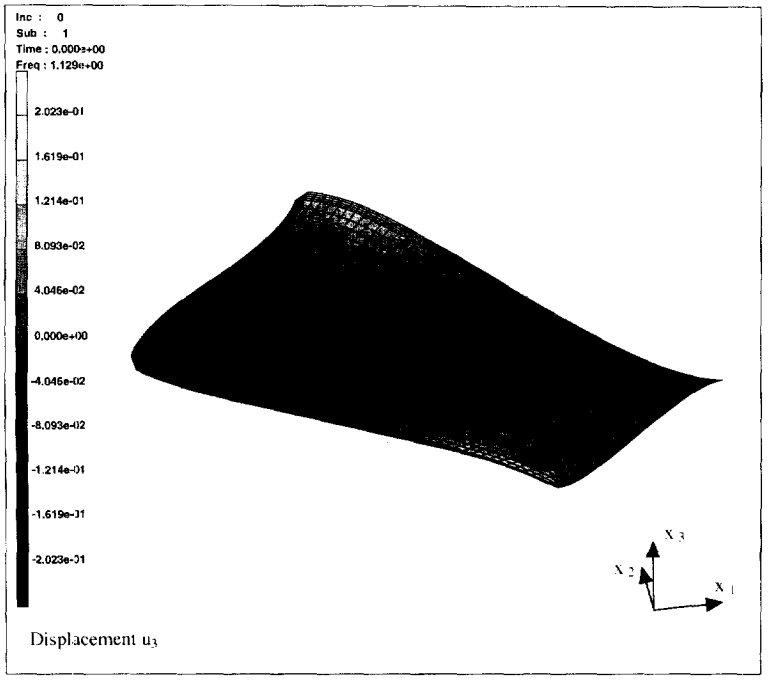

Fig. 6(d). The first torsional mode shape for the retrofitted column with the rectangular cross section.

by Toupin (1965), Knowles (1966), Horgan (1972), Choi and Horgan (1977), and Dong and Goetschel (1982) (see also a review article by Muki and Dong, 1993).

The displacement field (25) yields vanishing strains and stresses except ε_{23}, ε_{31}, σ_{23}, and σ_{31}. In order to define the boundary value problem over the cross section for the warping function, shear strains and stresses per unit angle of twist per axial length are introduced:

$$[2\varepsilon_{23} \quad 2\varepsilon_{31} \quad \sigma_{23} \quad \sigma_{31}]^{(\alpha)} = \psi_3 \cdot [2e_{23} \quad 2e_{31} \quad \tau_{23} \quad \tau_{31}]^{(\alpha)}. \tag{28}$$

Equations (3) and (4) with (5), (25), and (28) yield

$$\tau^{(\alpha)}_{13,1} + \tau^{(\alpha)}_{23,2} = 0 \quad \text{in}\,\Omega^{(\alpha)}, \tag{29}$$

$$\begin{Bmatrix} \tau_{23} \\ \tau_{31} \end{Bmatrix}^{(\alpha)} = \begin{bmatrix} C_{44} & C_{45} \\ C_{45} & C_{55} \end{bmatrix}^{(\alpha)} \begin{Bmatrix} w^{(\alpha)}_{,2} + x_1 \\ w^{(\alpha)}_{,1} - x_2 \end{Bmatrix} \quad \text{in}\,\Omega^{(\alpha)}, \tag{30}$$

where

$$C^{(\alpha)}_{44} = C^{(\alpha)}_{55} = G^{(\alpha)}, \quad C^{(\alpha)}_{45} = 0 \quad \text{for}\,\alpha = 1, 2. \tag{31}$$

By substituting (30) into (29), the equilibrium equation for the warping function becomes

$$C^{(\alpha)}_{55} w^{(\alpha)}_{,11} + 2C^{(\alpha)}_{45} w^{(\alpha)}_{,12} + C^{(\alpha)}_{44} w^{(\alpha)}_{,22} = 0 \quad \text{in}\,\Omega^{(\alpha)}. \tag{32}$$

The relevant boundary conditions consist of the continuity of the warping function and the traction in the x_3-direction on each interface between the steel bar and concrete, $\partial\Omega^{(1)}_m$:

$$w^{(1)} = w^{(2)}, \quad \tau^{(1)}_{j3} n^{(1)}_j = \tau^{(2)}_{j3} n^{(1)}_j \quad \text{on}\,\partial\Omega^{(1)}_m, \quad m = 0, 1, \ldots, N. \tag{33}$$

For retrofitted columns, the continuity conditions are also prescribed on the interface between the concrete and composite layer, $\partial\Omega^{(2)}_0$:

$$w^{(2)} = w^{(3)}, \quad \tau^{(2)}_{j3} n^{(2)}_j = \tau^{(3)}_{j3} n^{(2)}_j \text{on}\,\partial\Omega^{(2)}_0 \quad \text{if}\,\Omega^{(3)} \neq \varnothing. \tag{34a,b}$$

The traction free condition on the exterior composite surface, $\partial\Omega^{(3)}_0$ becomes:

$$\tau^{(3)}_{j3} n^{(3)}_j = 0 \quad \text{on}\,\partial\Omega^{(3)}_0 \quad \text{if}\,\Omega^{(3)} \neq \varnothing. \tag{34c}$$

For unretrofitted columns, the traction free condition holds on the boundary, $\partial\Omega^{(2)}_0$:

$$\tau^{(2)}_{j3} n^{(2)}_j = 0 \quad \text{on}\,\partial\Omega^{(2)}_0 \quad \text{if}\,\Omega^{(3)} = \varnothing. \tag{35}$$

Since the exterior boundary conditions, (34c) or (35), are a Neumann-type, w is determined up to an additive constant. In order to have a well-posed boundary value problem, the warping function is specified at the origin as:

$$w^{(2)} = 0 \quad \text{at}\,x_1 = x_2 = 0. \tag{36}$$

The minimum potential energy theorem furnishes a weak formulation of the problem (Herrmann, 1965):

$$\delta \left[\sum_{\alpha=1}^{3} \iint_{\Omega^{(\alpha)}} \frac{1}{2} [w^{(\alpha)}_{,2} + x_1 \quad w^{(\alpha)}_{,1} - x_2] \times \begin{bmatrix} C_{44} & C_{45} \\ C_{45} & C_{55} \end{bmatrix}^{(\alpha)} \begin{Bmatrix} w^{(\alpha)}_{,2} + x_1 \\ w^{(\alpha)}_{,1} - x_2 \end{Bmatrix} \mathrm{d}x_1\, \mathrm{d}x_2 \right] = 0. \tag{37}$$

The torsional rigidity is computed as

$$(GI_3)_{(e)} = \sum_{\alpha=1}^{3} \iint_{\Omega^{(\alpha)}} (x_1 \tau_{23}^{(\alpha)} - x_2 \tau_{31}^{(\alpha)})\, dx_1\, dx_2. \tag{38}$$

By utilizing the same mesh employed for the waveguide analyses, the warping function and torsional rigidity were computed using a finite element method (Herrmann, 1965).

It is noted that the boundary value problem defined by (29)–(36) has a unique solution. The existence and uniqueness of the solution can be proven by using the Lax–Milgram theorem for a coercive bilinear form derived from (37) after establishing the equivalence between the classical formulation (29)–(36) and the variational formulation (37) (see for example, Oden and Reddy, 1976; Brezzi and Gilard, 1987).

Tables 3 and 4, for RC columns before and after retrofitting, compare both the torsional rigidities and wave speed computed from the semi-inverse method, $(GI_3)_{(e)}$ and $C_{p(e)}$, with those from the elementary theory, $(GI_3)_{(m)}$ and $C_{p(m)}$. The torsional rigidity and wave speed were nondimensionalized by those of the monolithic concrete column with diameter d. Both tables show that the torsional rigidity obtained by the semi-inverse analysis with mass moment of inertia J_3 in (B4) accurately predicts the torsional wave speed, (B10), at the long wavelength limit. The errors in torsional rigidity predicted by the elementary theory are approximately 20% for both the circular and octagonal cross sections, 40% for the square cross section, and 70% for the rectangular cross section. The error increases with increasing warping, see Figs 4 and 6.

Due to the warping induced by reinforcing bars, the torsional rigidity predicted by the elementary theory is extremely inaccurate even for beams with circular cross sections. Therefore, it is necessary to compute the torsional rigidity according to (38) based upon the semi-inverse analysis in order to predict the dynamic torsional response of retrofitted RC columns.

The above observation was also confirmed by the analytical and experimental investigation conducted by Kuo and Conway (1973) for an epoxy cylinder with circular cross section reinforced by four brass bars. Kuo and Conway did not compare their results with the elementary theory. The elementary theory predicts the nondimensional ridigity of 4.98 for the composite beam. Kuo and Conway obtained the nondimensional torsional rigidity 1.57 analytically and 1.53 experimentally. The present FE analysis predicted 1.77. (This value was obtained from a coarse mesh of density similar to the mesh in Fig. 2 as well as a mesh four times finer than the coarse one.) Even though there is a slight difference between the analytical solution and the FE solution, the above observation is confirmed. it is noted

Table 3. Comparisons of nondimensional torsional rigidities and wave speed for the RC columns

	$\frac{(GI_3)_{(m)}}{G^{(2)}\pi/d^4/32}$	$\frac{(GI_3)_{(e)}}{G^{(2)}\pi d^4/32}$	$\frac{J_3}{\rho^{(2)}\pi d^4/32}$	$\frac{C_{p(m)}}{C_s^{(2)}}$	$\frac{C_{p(e)}}{C_s^{(2)}}$
Circle	1.28	1.06	1.09	1.08	0.99
Octagon	1.28	1.04	1.09	1.08	0.98
Square	1.34	0.93	1.14	1.09	0.91
Rectangle	1.48	0.86	1.24	1.09	0.84

Table 4. Comparisons of nondimensional torsional rigidities and wave speed for the retrofitted RC columns

	$\frac{(GI_3)_{(m)}}{G^{(2)}\pi d^4/32}$	$\frac{(GI_3)_{(e)}}{G^{2}\pi d^4/32}$	$\frac{J_3}{\rho^{(2)}\pi d^4/32}$	$\frac{C_{p(m)}}{C_s^{(2)}}$	$\frac{C_{p(e)}}{C_s^{(2)}}$
Circle	1.36	1.14	1.22	1.05	0.97
Octagon	1.37	1.14	1.23	1.06	0.96
Square	1.50	1.07	1.36	1.05	0.89
Rectangle	1.59	0.95	1.41	1.06	0.82

that Kuo and Conway's solution was obtained by truncating a stress function expressed in a double infinite series. An analytical and experimental investigation on torsional rigidity of RC columns with circular cross sections will be deferred to a subsequent publication.

CONCLUSIONS

In order to investigate the changes in torsional wave velocities of RC columns due to composite retrofitting, waveguide analyses were conducted for RC columns with circular, octagonal, square, and rectangular cross sections of equal area. Comparisons of the phase velocity spectra between the columns with and without exterior composite layers show that the retrofitted columns have slightly smaller phase velocity of the first torsional mode. The first mode shapes exhibit marked warping induced by vertical bars.

Comparisons of the phase velocity of the first torsional mode with those predicted by elementary theories indicate that the elementary theory does not accurately predict the torsional wave speed even at the long wavelength limit. However, the elementary theory can predict torsional wave speed if the torsional rigidity was computed by utilizing Saint-Venant's semi-inverse method for torsional warping.

Acknowledgement—A pre- and post-processor, MENTAT, developed by MARC Analysis Research Corporation was utilized for mesh generation and post processing—the authors are thankful to Mr. Reza Sadegi for his software support. The authors are thankful to Mr. San Le for assisting in the preparation of the manuscript.

REFERENCES

Armenakas, A. E. (1965) Torsional waves in composite rods. *The Journal of the Acoustical Society of America* **38**(3), 439–446.

Bancroft, D. (1941) The velocity of longitudinal waves in cylindrical bars. *Physical Review* **59**(4), 588–593.

Barr, A. D. S. (1962) Torsional waves in uniform rods of non-circular section. *Journal of Mechanical Engineering Science* **4**(2), 127–135.

Brezzi, F. and Gilardi, G. (1987) Functional analysis (Chap. 1), Functional spaces (Chap. 2). In *Finite Element Handbook*, ed. H. Kardestuncer, pp. 1.3–1.76. McGraw-Hill Book Company, New York, N.Y.

Choi, I. and Horgan, C. O. (1977) Saint-Venant's principle and edge effects in anisotropic elasticity. *ASME Journal of Applied Mechanics* **44**(3), 424–430.

Chree, C. (1889) The equations of an isotropic elastic solid in polar and cylindrical coordinates, their solutions and applications. *Transactions of the Cambridge Philosophical Society* **14**, 250–369.

Davies, R. M. (1956) Stress waves in solids. *Surveys in Mechanics*, ed. Batchelor, G. K. and Davies, R. M., pp. 64–138. Cambridge University Press.

Dong, S. B. and Goetschel, D. B. (1982) Edge effects in laminated composite plates. *ASME Journal of Applied Mechanics* **49**(1), 129–135.

Fung, Y. C. (1965) *Foundation of Solid Mechanics*. Prentice-Hall, Englewood Cliffs, NJ.

Gazis, D. C. (1959) Three-dimensional investigation of the propagation of waves in hollow circular cylinders. I. Analytical foundation. *The Journal of the Acoustical Society of America* **31**(5), 568–573.

Haines, D. W. and Lee, P. C. Y. (1971) Axially symmetric torsional waves in circular composite cylinders. *ASME Journal of Applied Mechanics* **38**(4), 1042–1044.

Herrmann, L. R. (1965) Elastic torsional analysis of irregular shapes. *ASCE Journal of the Engineering Mechanics Division* **91**(EM6), 11–19.

Horgan, C. O. (1972) On Saint-Venant's principle in plane anisotropic elasticity. *Journal of Elasticity* **2**(3), 169–180.

Hughes, T. J. R. (1987) *The Finite Element Method, Linear Static and Dynamic Finite Element Analysis*, Prentice-Hall, Englewood Cliffs, NJ.

Kaul, R. K., Shaw, R. P. and Muller, W. (1981) Torsional waves in an axially homogeneous bimetallic cylinder. *International Journal of Solids and Structures* **17**(4), 379–394.

Knowles, J. K. (1966) On Saint-Venant's principle in the two-dimensional linear theory of elasticity. *Archive for Rational Mechanics and Analysis* **21**(1), 1–22.

Kuo, Y. M. and Conway, H. D. (1973) The torsion of composite tubes and cylinders. *International Journal of Solids and Structures* **9**(12), 1553–1566.

Lekhnitskii, S. G. (1963) *Theory of Elasticity of Anisotropic Elastic Body*, translated by P. Fern. Holidan-Day, San Francisco.

Love, A. E. H. (1944) *Treatise on the Mathematical Theory of Elasticity*, 4th edn. Dover Publishing, New York, N.Y.

Mason, W. E., Jr. and Herrmann, L. R. (1968) Elastic shear analysis of general prismatic beams. *ASCE Journal of the Engineering Mechanics Division* **94**(EM4), 965–983.

Muki, R. and Dong, S. B. (1993) Recent advances in Saint-Venant's solutions and principles (in Japanese). *Transactions of the Japan Society of Mechanical Engineers* **59**(559), 512–517.

Nelson, R. B., Dong, S. B. and Kalra, R. D. (1971) Vibration and waves in laminated orthotropic circular cylinders. *Journal of Sound and Vibration* **18**(3), 429–444.

Noble, B. and Daniel, J. W. (1977) *Applied Linear Algebra*, Chap. 9. Prentice-Hall, Englewood Cliffs, NJ.

Oden, J. T. and Reddy, J. N. (1976) *An Introduction to the Mathematical Theory of Finite Elements*, Chap. 7. John Wiley and Sons, New York, N.Y.
Owen, J. D. (1950) Ph.D. thesis, University of Wales.
Rattanawangcharoen, N., Shah, A. H. and Datta, S. K. (1992) Wave propagation in laminated composite circular cylinders. *International Journal of Solids and Structures* **29**(6), 767–781.
Reuter, R. C., Jr. (1969) First-branch dispersion of torsional waves in bimaterial rods. *The Journal of the Acoustical Society of America* **46**(3), 821–823.
Saint-Venant, A.-J.-C. Barre De (1856) Memoire sur la torsion des prismes. *Mem. Savants Etrangers* **14**, 233–560.
Timoshenko, S. and Goodier, J. N. (1951, 1970). *Theory of Elasticity*, 3rd edn. McGraw-Hill Publishing Co., New York.
Toupin, R. A. (1965) Saint-Venant's principle. *Archive for Rational Mechanics and Analysis* **18**(1), 83–96.

APPENDIX A: BASIC EQUATIONS FOR THE FE IMPLEMENTATION

A typical finite element region $\Gamma^{(e)}$ is defined by a coordinate map from the standard square region in the ξ, η-plane, $|\xi| \leqslant 1$, $|\eta| \leqslant 1$. The corner points are identified by nodes, 1–4 in the counterclockwise direction. These nodal coordinates in the standard region are, beginning from node 1, $(-1,-1)$, $(1,-1)$, $(1,1)$, $(-1,1)$. For notational simplicity, node numbers are denoted by hatted integers, $\hat{i} = 1$–4. The shape functions, employed for both coordinate and displacement mappings, are defined as:

$$N_{\hat{i}} = \tfrac{1}{4}(1+\xi_{\hat{i}}\xi)(1+\eta_{\hat{i}}\eta), \tag{A1}$$

where

$$(\xi_{\hat{i}}, \eta_{\hat{i}}), \quad i = 1-4,$$

are the above nodal coordinates.

The interpolation matrix $[N]$ and nodal displacement vector are defined as:

$$\{\tilde{u}\} = [N]\{\tilde{U}\} = \sum_{\hat{i}=1}^{4} \begin{bmatrix} N_{\hat{i}} & 0 & 0 \\ o & N_{\hat{i}} & 0 \\ 0 & 0 & N_{\hat{i}} \end{bmatrix} \begin{Bmatrix} \tilde{U}_1^{\hat{i}} \\ \tilde{U}_2^{\hat{i}} \\ \tilde{U}_3^{\hat{i}} \end{Bmatrix}, \tag{A2}$$

where $\tilde{U}_j^{\hat{i}}$ is the jth displacement component at node $\hat{i}$.

The strain–displacement matrix is defined as:

$$\{\tilde{\varepsilon}\} = [B]\{\tilde{U}\} = \sum_{\hat{i}=1}^{4} \begin{bmatrix} N_{\hat{i},1} & 0 & 0 \\ 0 & N_{\hat{i},2} & 0 \\ 0 & 0 & \sqrt{-1}kN_{\hat{i}} \\ 0 & \sqrt{-1}kN_{\hat{i}} & N_{\hat{i},2} \\ \sqrt{-1}kN_{\hat{i}} & 0 & N_{\hat{i},1} \\ N_{\hat{i},2} & N_{\hat{i},1} & 0 \end{bmatrix} \begin{Bmatrix} \tilde{U}_1^{\hat{i}} \\ \tilde{U}_2^{\hat{i}} \\ \tilde{U}_3^{\hat{i}} \end{Bmatrix}. \tag{A3}$$

The composite layer is cylindrically orthotropic with one of the material axes aligned in the x_3-direction. Therefore, with respect to the x_1, x_2, x_3-coordinate system, the composite layer is characterized as a monoclinic material with a single plane of symmetry, x_3 = constant (Lekhnitskii, 1963).

The elastic modulus matrix for monoclinic materials becomes:

$$[D]^{(\alpha)} = \begin{bmatrix} C_{11} & C_{12} & C_{13} & 0 & 0 & C_{16} \\ C_{12} & C_{22} & C_{23} & 0 & 0 & C_{26} \\ C_{13} & C_{23} & C_{33} & 0 & 0 & C_{36} \\ 0 & 0 & 0 & C_{44} & C_{45} & 0 \\ 0 & 0 & 0 & C_{45} & C_{55} & 0 \\ C_{16} & C_{26} & C_{36} & 0 & 0 & C_{66} \end{bmatrix}^{(\alpha)}, \tag{A4}$$

where for isotropic steel ($\alpha = 1$) and concrete ($\alpha = 2$) the above moduli are expressed in terms of Young's modulus and Poisson's ratio:

$$C_{11}^{(\alpha)} = C_{22}^{(\alpha)} = C_{33}^{(\alpha)} = \left\{\frac{E(1-\nu)}{(1+\nu)(1-2\nu)}\right\}^{(\alpha)}, \quad C_{12}^{(\alpha)} = C_{13}^{(\alpha)} = C_{23}^{(\alpha)} = \left\{\frac{\nu E}{(1+\nu)(1-2\nu)}\right\}^{(\alpha)},$$

$$C_{44}^{(\alpha)} = C_{55}^{(\alpha)} = C_{66}^{(\alpha)} = \left\{\frac{E}{2(1+\nu)}\right\}^{(\alpha)}, \quad C_{16}^{(\alpha)} = C_{26}^{(\alpha)} = C_{36}^{(\alpha)} = C_{45}^{(\alpha)} = 0, \quad \alpha = 1, 2. \tag{A5}$$

APPENDIX B: ELEMENTARY RC TORSION EQUATIONS

Let the angle of twist of a cross section be denoted by $\Psi_3(x_3, \omega)$. Assuming that cross sections remain plane during deformation, i.e., no warping, the displacement field in the beam (column) is approximated as:

$$u_1(x_1, x_2, x_3, \omega) \approx -\Psi_3(x_3, \omega)x_2, u_2(x_1, x_2, x_3, \omega) \approx \Psi_3(x_3, \omega)x_1, \quad u_3(x_1, x_2, x_3, \omega) \approx 0. \tag{B1}$$

The torque is defined in terms of the stresses as:

$$M_3 = \iint_{\Omega} (x_1\sigma_{32} - x_2\sigma_{31})\,\mathrm{d}x_1\,\mathrm{d}x_2. \tag{B2}$$

The elementary torsion equation in the frequency domain becomes

$$M_{3,3} + \omega^2 J_3 \Psi_3 = 0. \tag{B3}$$

Where J_3 is the polar mass moment of inertia:

$$J_3 = \iint_{\Omega} \rho(x_1^2 + x_2^2)\,\mathrm{d}x_1\,\mathrm{d}x_2. \tag{B4}$$

It is noted that for harmonic wave (free vibration) analyses, external couples are absent.

In the elementary theory, a torsional stress state, $\sigma_{31} \neq 0$ and $\sigma_{32} \neq 0$, is assumed. The resulting Hooke's law becomes

$$\sigma_{11}^{(\alpha)} = \sigma_{22}^{(\alpha)} = \sigma_{33}^{(\alpha)} = \sigma_{12}^{(\alpha)} = 0, \sigma_{32}^{(\alpha)} = C_{44}^{(\alpha)}(u_{3,2}^{(\alpha)} + u_{2,3}^{(\alpha)}) + C_{45}^{(\alpha)}(u_{3,1}^{(\alpha)} + u_{1,3}^{(\alpha)}), \quad \sigma_{31}^{(\alpha)} = C_{45}^{(\alpha)}(u_{3,2}^{(\alpha)} + u_{2,3}^{(\alpha)}) + C_{55}^{(\alpha)}(u_{3,1}^{(\alpha)} + u_{1,3}^{(\alpha)}), \tag{B5}$$

where C_{ij} is the compact notation of the elastic modulus tensor, as defined in (A4) of Appendix A.

By computing (B5) with the strains computed from (B1) and substituting this into (B2), a constitutive relation is obtained as:

$$M_3 = (GI_3)_{(m)}\Psi_{3,3}, \tag{B6}$$

where the torsional rigidity of the beam is defined as:

$$(GI_3)_{(m)} = \iint_{\Omega} (C_{44}x_1^2 + C_{55}x_2^2)\,\mathrm{d}x_1\,\mathrm{d}x_2. \tag{B7}$$

In evaluating the above integration over the cross section, both the steel and composite sub-regions must be properly accounted for. In the above, it is assumed that

$$\iint_{\Omega} C_{45}x_1x_2\,\mathrm{d}x_1\,\mathrm{d}x_2 = 0,$$

which holds for the cross sections with double axes of symmetry.

The torsion equations consist of the equations of motion, (B3), and the constitutive equation (B6). The equation of motion for torsion is rewritten in terms of the angle of twist by substituting (B6) into (B3). Next the harmonic wave form in the x_3-direction is assumed:

$$\Psi_3 = \tilde{\Psi}_3 \exp(\sqrt{-1}kx_3). \tag{B8}$$

The substitution (B8) into the equation of motion for the angle of twist furnishes

$$\{-k^2(GI_3)_{(m)} + J_3\omega^2\}\tilde{\Psi}_3 = 0. \tag{B9}$$

For torsional motion,

$$C_p = \sqrt{\frac{(GI_3)_{(m)}}{J_3}}. \tag{B10}$$

For torsional wave motion, the elementary theory predicts a nondispersive phase velocity spectrum.